J Mater Sci (2008) 43:7141–7147
DOI 10.1007/s10853-008-3028-9

Structure characterization of hydration products generated by alkaline activation of granulated blast furnace slag

Yao Jun Zhang · Yong Lin Zhao · Hai Hong Li · De Long Xu

Received: 1 June 2008 / Accepted: 30 September 2008 / Published online: 24 October 2008

Abstract The hydration mechanism and mineral phase structures by waterglass activation of granulated blast furnace slag (GBFS) are investigated in detail by means of XRD and FTIR. The results show that the network structures of glassy phases are disintegrated and there is not any new material phase formed in the early stage of hydration processes. With evolution of hydration, the polycondensation reaction takes place between $[SiO_4]^{4-}$ and $[AlO_4]^{5-}$ species and some new mineral phases are produced. A hydration mechanism for the formation of geopolymer by waterglass activation of GBFS is proposed in detail.

Introduction

The shortage of limestone reserves and CO_2 release in the manufacture of ordinary Portland cement (OPC) have promoted the researchers to explore some new building materials for the sustainable development of concrete industry[1]. Glukhovsky and subsequently Krivenko developed alkali-activated systems, containing calcium silicate hydrate (CSH) and aluminosilicate phases in the 1950s [2–5]. The geopolymer, as an alkaline aluminosilicate cementitious material, has been extensively investigated in recent years due to its excellent mechanical characteristics and potential commercial applications including high compressive strength; durability; acid-resistant; fire-resistance; and immobilization of toxic, hazardous, and radioactive wastes [6–9]. The raw materials for synthesis of geopolymers have focused on making use of metakaolin clay and industrial wastes of coal fly ash and metallurgical slag to produce high added value products and minimize environmental impacts [7, 10]. Krivenko and Kovalchuk [11] reported that the alkaline activation of metakaolin- and fly ash-based geocements having zeolite-like structure in a crystalline or semi-crystalline state exhibited a highly heat resistant characteristic. Synthesis of geopolymer is based on activation of aluminosilicate in wastes by an alkali metal hydroxide or an alkali metal salt to produce Si–O–Al three-dimensional inorganic amorphous structures [12]. It is known that the production of geopolymer requires around 60% less energy and less CO_2 emissions compared to ordinary Portland cement. The manufacture of geopolymer by alkaline activation of granulated blast furnace slag has been paid much attention at present [10, 13–19]. Generally, the geopolymerization involves two steps of chemical reactions, that is, dissolution of raw materials and polycondensation to form Si–O–Al network structures [12]. However, the exact mechanism of polymerization is not yet well understood up to now.

Here, the geopolymer is prepared by alkaline activation of an industrial waste of granulated blast furnace slag (GBFS). The microstructures and chemical bonding properties of the hydration products are studied by means of X-ray diffraction (XRD) and Fourier transform infrared spectroscopy (FTIR). A desirable mechanism, especially for the formation of mineral phases in the hydration process, is first proposed in detail to our knowledge.

Y. J. Zhang (✉) · Y. L. Zhao · H. H. Li · D. L. Xu
College of Material Science and Engineering, Xi'an University of Architecture and Technology, Xi'an 710055, People's Republic of China
e-mail: yaojzhang@yahoo.com.cn

Table 1 Chemical composition of GBFS (wt%)

Chemical composition	SiO_2	CaO	Al_2O_3	MgO	TiO_2	MnO	Na_2O	K_2O	SO_3	Loss
Wt%	32.40	38.90	13.90	9.31	0.89	0.07	0.30	0.54	2.76	<0.8

Experimental

Materials

The GBFS used for synthesis of geopolymer is obtained from Taiyuan steel company in China. The major components of GBFS in mass percentage are listed in Table 1 and the Blaine specific surface area is 701 m^2/kg. A chemical reagent, sodium metasilicate $Na_2SiO_3 \cdot 9H_2O$ (Shanghai Chemical Reagent Co., 98% purity), is used as an alkali activator with waterglass modulus of 1.0.

Preparation of geopolymer paste

Raw material was blended in the ratio of waterglass: GBFS: water = 1:9:2.5 (in weight). The paste was cast into 50 (length) × 31.6 (width) × 31.6 (height) (mm^3) metal model. After demolding, a triplicate set of samples were put in a curing box at 20 °C with 99% relative humidity and the curing time was 0.5 h, initial setting time,final setting time,1 day (1d), 3 days (3d), 7 days (7d), and 28 days (28d), respectively. The compressive strengths of samples were determined and then the samples were simultaneously used for analysis by X-ray diffraction and Fourier transform infrared spectroscopy.

Characterization of geopolymer

The X-ray diffraction (XRD) patterns of geopolymers were carried out on an X'Pert PRO MPD diffractometer using CuKα irradiation with a 0.04° 2θ step interval and working electric current of 40 mA and voltage of 40 KV. The Fourier transform infrared spectra of samples were measured using a Nicolet 5700 spectrometer with standard KBr technique. About 0.5 mg sample mixed with 250 mg KBr was pressed into pellets.

Results and discussion

Structure characterizations of geopolymer and mineral phases

Figure 1 shows the XRD patterns of samples by waterglass activation of GBFS. From the pattern of GBFS it can be observed that there is a broad diffuse hump peak in the region 20–38° 2θ suggesting that the GBFS predominantly

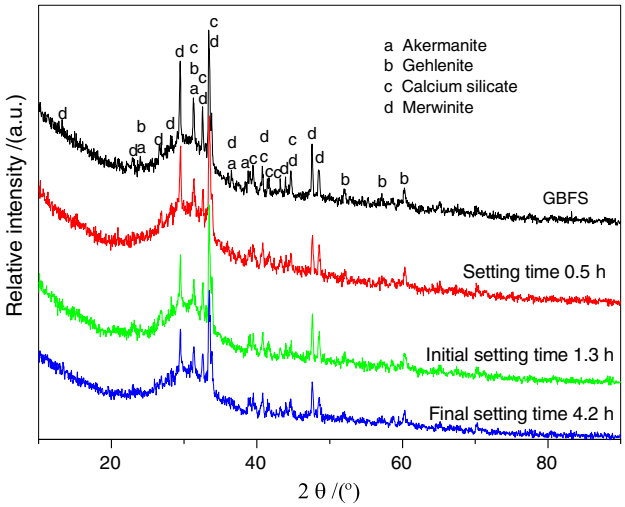

Fig. 1 XRD patterns of samples by waterglass activation of GBFS. The curve of GBFS, setting time for 0.5 h, initial time for 1.3 h and final setting time for 4.2 h, respectively

consists of glassy phases [6–8]. Besides, there are four kinds of mineral phases, akermanite, gehlenite, calcium silicate, and merwinite, and their chemical composites as well as d values are listed in Table 2. In comparison to the pattern of GBFS, the relative intensities of diffraction peaks have no distinct changes and have no new peak appearance from setting time for 0.5 h to final setting time for 4.2 h in Fig. 1 implying that sodium hydroxide deriving from the hydrolysis of waterglass promotes some vitreous dissolution in the periods of curing ages.

The XRD patterns of samples for curing ages 1d, 3d, 7d, 28d and steam curing time of 28d are displayed in Fig. 2. After the curing time of 1d, the intensities of some diffraction peaks remarkably decrease and some peaks disappear in comparison to final setting time in Fig. 1 demonstrating that those crystal phases, either partial or whole, dissolve into aqueous sodium hydroxide solution derived from the hydrolysis of waterglass [20]. It is noteworthy that some new phases, tobermolite and calcium silicate hydrate (CSH) gel, are generated during curing time of 1d. Schneider et al [21] reported that the CSH and other hydrated phases are present in hardened pastes of alkali-activated blast furnace slag. Some new mineral phases are simultaneously produced at later curing times, for instance, gismondine in 3d, zoisite in 7d, wairakite and natrolite in 28d, clinozoisite in steam curing time of 28d. The chemical composites of these mineral phases and

Table 2 Mineral phases of samples by waterglass activation of GBFS from initial setting time to final setting time

Mineral phase	Chemical formula	Number of JCPDS	d/nm
Akermanite	$Ca_2MgSi_2O_7$	01-087-0049	0.37148, 0.28593, 0.24635, 0.23078
Gehlenite	$Ca_2Al_2SiO_7$	01-089-5917	0.37148, 0.28593, 0.17589, 0.16100, 0.15347
Calcium silicate	Ca_2SiO_4	00-033-0303	0.28593, 0.27520, 0.26840, 0.22836, 0.22140, 0.21772, 0.20913, 0.20282
Merwinite	$Ca_3Mg(SiO_4)_2$	00-026-1064	0.66288, 0.387703, 0.33578, 0.31639, 0.30332, 0.27520, 0.26840, 0.24635, 0.22140, 0.20596, 0.20282, 0.19094, 0.18774

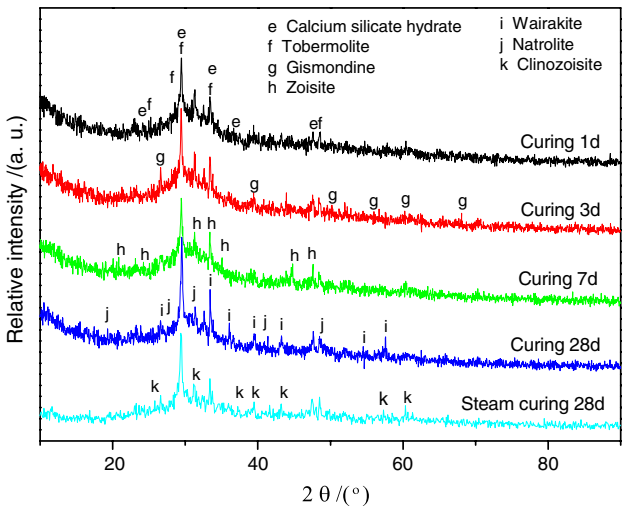

Fig. 2 XRD patterns of samples by waterglass activation of GBFS in the period of curing times 1–28d

d values are listed in Table 3. Meanwhile, it can be observed that the hump peak in the range of 20–38° 2θ hardly changes in the period of curing time of 1d to steam curing time of 28d, suggesting that geopolymer gel and calcium silicate hydrate (CSH) gel produced coexist in the pastes [17]. Indeed, once GBFS powder is mixed with the alkaline solution, geopolymer gel and CSH gel could be formed after shorter setting and hardening times. As there is no sufficient time for the gel in pastes to grow into a well crystallized structure the hump peak was generated in the period of 1–28d in Fig. 2. The geopolymer exhibits

Table 4 Compressive strength of geopolymer

Compressive strength (MPa)			
1d	3d	7d	28d
26.5	40.7	51.6	60.1

increasing mechanical properties as shown in Table 4. Yip et al [15] described that it could be able to produce Na-geopolymer gel, Ca-geopolymer gel, and CSH gel in a metakaolin/GGBFS system.

Figure 3 illustrates the FTIR spectra of samples by waterglass activation of GBFS in the period of initial to final setting times. The characteristic bands at around 947.3 cm^{-1} and 697 cm^{-1} are assigned to asymmetric Si–O–Al stretching mode and symmetric stretching vibrations of Si–O–Si and Si–O–Al bonds [16]. The asymmetric Si–O–Al stretching vibration is shifted from 997 cm^{-1} at setting time for 0.5 h in Fig. 3b to 1017.2 cm^{-1} at final setting time for 4.2 h in Fig. 3d. The wavenumber of 1017.2 cm^{-1} is ascribed to asymmetric Si–O–Si stretching mode [22] because the hydrolysis of glasswater to produce different aggregates of silica gel which are composed of $[SiO_4]^{4-}$ monomers, $[Si_2O_7]^{6-}$ dimmer, $[Si_3O_{10}]^{8-}$ trimer, and some oligomer species [23]. The band at around 1435 cm^{-1} from Fig. 3a–d is attributed to the absorption of C–O stretching vibration due to carbonation formed in atmosphere [24]. Both 1632 cm^{-1} and 3445 cm^{-1} are assigned to bending and stretching vibration of hydroxyl groups existing in various hydration products [25].

Table 3 Mineral phases of samples by waterglass activation GBFS in the period of curing time 1–28d

Mineral phase	Chemical formula	Number of JCPDS	d/nm
Calcium silicate Hydrate	$Ca_2SiO_4 \cdot 0.3H_2O$	00-015-0584	0.36650, 0.30326(s), 0.26810, 0.24572, 0.19106
Tobermolite	$Ca_5(Si_6O_{16})(OH)_2$	01-089-6458	0.35642, 0.31152, 0.30326(s), 0.26810, 0.18760
Gismondine	$CaAl_2Si_2O_8 \cdot 4H_2O$	00-020-0452	0.33499(s), 0.13782, 0.18174, 0.16406, 0.15426, 0.13750
Zoisite	$Ca_2Al_3Si_3O_{12}OH$	01-078-1247	0.42538, 0.36951, 0.28585(s), 0.26836, 0.25602, 0.20277, 0.19110
Wairakite	$CaAl_2Si_4O_{12} \cdot 2H_2O$	00-042-1451	0.33878(s), 0.26800, 0.24904, 0.22792, 0.20895, 0.16821, 0.16011
Natrolite	$Na_2Al_2Si_3O_{10} \cdot 2H_2O$	00-022-1224	0.45987, 0.31576, 0.28506(s), 0.21835, 0.18769
Clinozoisite	$Ca_2Al_3Si_3O_{12}OH$	00-016-0705	0.34555, 0.28664(s), 0.24101, 0.22805, 0.20895, 0.1600, 0.15353

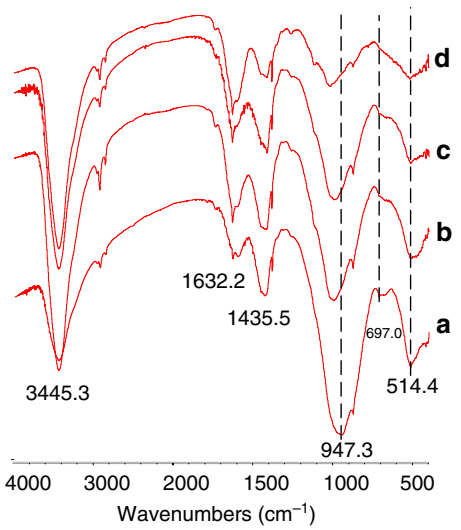

Fig. 3 FTIR spectra of samples by waterglass activation of GBFS from initial to final setting times. (a) GBFS, (b) alkali activation of GBFS for 0.5 h, (c) initial setting time for 1.3 h and (d) final setting time for 4.2 h

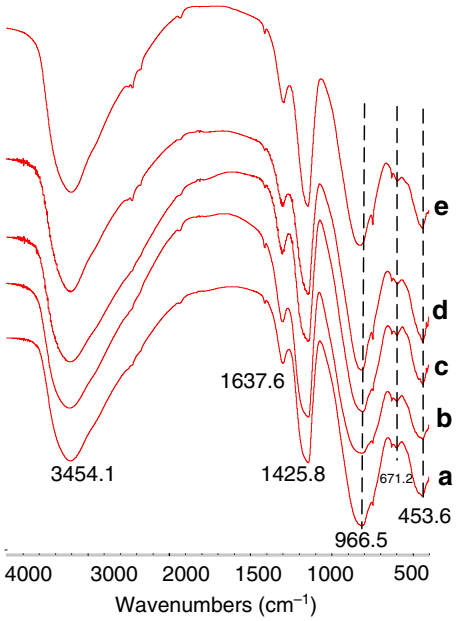

Fig. 4 FTIR spectra of samples by waterglass activation of GBFS in periods of curing times 1–28d. (a) Curing time of 1d, (b) curing time of 3d, (c) curing time of 7d, (d) curing time of 28d and (e) steam curing time of 28d

Figure 4 shows the FTIR spectra of the samples in the curing time from 1d to 28d. It can be clearly seen that the stretching vibration of Si–O–Al bonds is gradually shifted to high wavenumber from 966.5 cm^{-1} at curing time of 1d in Fig. 4a to 981.5 cm^{-1} at steam curing time of 28d in Fig. 4e, considering that the polymeric matrix is growing and accompanies the increase of the compressive strength shown in Table 4.

In comparison to final setting time in Fig. 3d, two kinds of new bands appearing in the region 671.2 and 714.0 cm^{-1} belong to the symmetric absorption of Si–O–Si and Al–O–Si bonds, and the relative intensities hardly changes from Fig. 4a to d. It is demonstrated that the partial of $[SiO_4]^{4-}$ units within the Si–O–Si skeleton are replaced by $[AlO_4]^{5-}$ to form geopolymer gel and have relatively stable Si/Al ratio in Si–O–Al network skeleton [26].

Hydration mechanism

From the XRD and FTIR results, the hydration mechanism for geopolymer formed by waterglass activation of GBFS can be schematically described as below:

Hydrolysis of waterglass

When solid waterglass is mixed with water, the hydrolysis takes place immediately and produces orthosilicic acid and sodium hydroxide shown in reaction (1).

$$2Na_2SiO_3 + 6H_2O \rightarrow 2Si(OH)_4 + 4NaOH \quad (1)$$

Disintegration of glassy network structure

Under alkaline conditions, the covalent Si–O–Si, Si–O–Al, and Al–O–Al bonds in the vitreous phases of the GBFS are broken to form aluminum hydroxide and orthosilicic acid as shown in reaction (2). Higher concentration of hydroxyl ions facilitate the dissociation of different silicate and aluminate species, and then these species further react with NaOH to produce the basic sodium aluminate and basic sodium silicate in reactions (3) and (4). The Al species consists of $[Al(OH)_4]^-$ and $[AlO(OH)_3]^{2-}$, while the Si species predominantly exists in the form of $Si(OH)_4$ and $[SiO(OH)_3]^-$ under alkaline conditions [27]. In this reaction stage, the speed of monomer formation is greater than that of the precipitation formation [15].

$$\dagger\text{O-Si(O)(O)-O-Al}^{-}\text{(O)-O-Si(O)(O)-O}\ddagger_n + nH_2O \xrightarrow{NaOH} nAl^{-}(OH)_4 + 2nSi(OH)_4 \quad (2)$$

$$^{-}Al(OH)_4 + NaOH \rightarrow Na^{+}[OAl^{-}(OH)_3]^{-} + H_2O \quad (3)$$

$$Si(OH)_4 + NaOH \rightarrow Na^{+}[OSi(OH)_3]^{-} + H_2O \quad (4)$$

Production of geopolymers

The polymeric structure of Si–O–Al skeleton can be restructured by means of intermolecular polycondensation

which is usually via a nucleophilic addition–elimination reactions between $[OSi(OH)_3]^-$ and $[OAl(OH)_3]^{2-}$ species under the alkaline condition. The hydroxyl group of $[OSi(OH)_3]^-$ attacks Al ion of $[OAl(OH)_3]^{2-}$ which results in a nucleophilic addition reaction to produce an intermediate complex [27]. Two hydroxyl groups in the intermediate complex eliminate a H_2O molecule to form a chain-like geopolymer via an elimination reaction shown in reaction (5). Further, an amorphous three-dimensional aluminosilicate network structure can be restructured by polycondensation of eliminating H_2O between the chain-like geopolymers with alkaline cations compensating the deficit charges described in reaction (6). In general, it can be affirmed that the OH^- ion acts as a catalyst [8]. According to Davidovits's reports, the geopolymers having amorphous to semi-crystalline three-dimensional aluminosilicate structures were divided into the polysialate (Si–O–Al–O–), the polysialate-siloxo (Si–O–Al–O–Si–O–) and the polysialate-disiloxo (Si–O–Al–O–Si–O–Si–O–) [12].

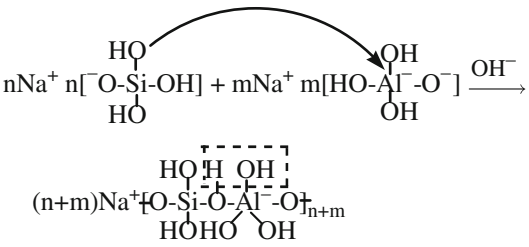

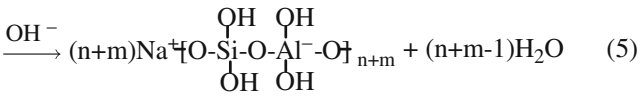

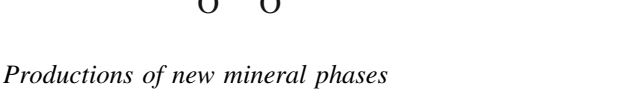

$$(n+m)Na^+[O\text{-}Si\text{-}O\text{-}Al^-\text{-}O]_{n+m} + (n+m-1)H_2O \quad (6)$$

Productions of new mineral phases

NaOH from the hydrolysis of waterglass increases the alkalinity in geopolymer paste. In such a case, the oligomers arising from the cleavages of glassy network structure consisting of SiO_4 and AlO_4 tetrahedron react with Ca^{2+} and Na^+ ions to produce the new mineral phases under the alkaline condition.

(1) Production of calcium silicate hydrate The siliceous species could exist in the form of $[(HO)_2SiO_2]^{2-}$ and $[HOSiO_3]^{3-}$ under highly alkaline conditions so that the $[(HO)_3SiO]^-$ anion from reaction (4) further reacts with OH^- ion to produce the species shown in reactions (7) and (8) [22, 28]. A new phase, calcium silicate hydrate (CSH), is generated by the reaction of Ca^{2+}, $HOSiO_3{}^{3-}$ and OH^- ions described in reaction (9).

$$[(HO)_3SiO]^- + OH^- \rightarrow [(HO)_2SiO_2]^{2-} + H_2O \quad (7)$$

$$[(HO)_2SiO_2]^{2-} + OH^- \rightarrow [(HO)SiO_3]^{3-} + H_2O \quad (8)$$

$$Cd^{2+}[(HO)SiO_3]^{3-} + OH^- \rightarrow CaSiO_4H_2O \quad (9)$$

(2) Production of tobermolite Under the alkali catalysis, two molecular $[(HO)_3SiO]^-$ and four molecular $[(HO)_2SiO_2]^{2-}$ undergo polycondensation to produce hexamer in reaction (10), and then it further reacts with Ca^{2+} to generate tobermolite as shown in reaction (11). Feng et al. [23] reported that the glassy structure reacts with OH^- not only to produce the ions of $[(HO)_3SiO]^-$, $[(HO)_2SiO_2]^{2-}$ and $[HOSiO_3]^{3-}$, but also to give rise to various oligomers.

$$[(HO)_3SiO]^- + 4[(HO)_2SiO_2]^{2-} + [(HO)_3SiO]^- \xrightarrow{OH^-}$$

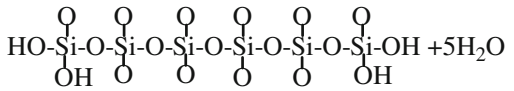

(10)

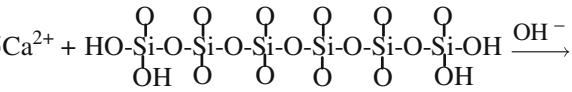

$$Ca_5Si_6O_{16}(OH)_2 + H_2O \quad (11)$$

(3) Production of gismondine Polycondensation of two molecular $Si(OH)_4$ and two molecular $Al^-(OH)_4$ loses H_2O and gains a tetramer containing silicon and aluminum under the alkali catalysis depicted in reaction (12), and then the tetramer reacts with Ca^{2+} to lose H_2O and produce gismondine in reaction (13). Weng and Sagoe-Crentsil [27] reported that the condensation reaction takes place between $Al^-(OH)_4$ and $[(HO)_3SiO]^-$ species.

$$2Si(OH)_4 + 2Al^-(OH)_4 \xrightarrow{OH^-}$$

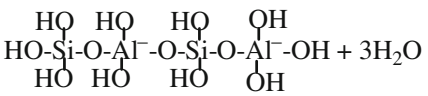

(12)

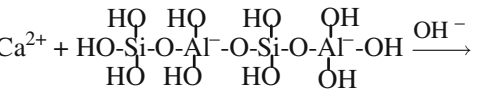

$$Ca_2Al_2Si_2O_8\ 4H_2O + H_2O \quad (13)$$

(4) Production of zoisite One molecular $[(HO)_3SiO]^-$, one molecular $Al^-(OH)_4$, and two molecular $Si(OH)_4$ undergo polycondensation to eliminate water and obtain hexamer shown in reaction (14), and then the hexamer

reacts with Ca^{2+} to produce zoisite shown in reaction (15).

$$[(HO)_3SiO]^- + 3Al^-(OH)_4 + 2Si(OH)_4 \xrightarrow{OH^-}$$

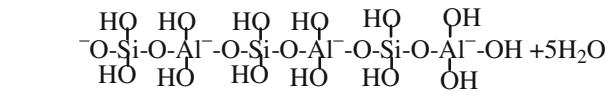

$$+ 5H_2O \quad (14)$$

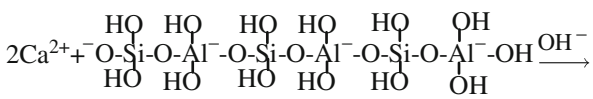

$$Ca_2Al_3Si_3O_{12}OH + 6H_2O \quad (15)$$

(5) Production of wairakite A number of six molecules, $4Si(OH)_4$ and $2Al^-(OH)_4$, reacts with each other to produce hexamer containing silicon and aluminum in reaction (16), and then the hexamer sequentially reacts with Ca^{2+} to produce wairakite in reaction (17).

$$4Si(OH)_4 + 2Al^-(OH)_4 \xrightarrow{OH^-}$$

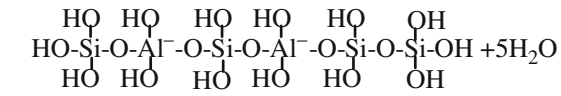

$$+ 5H_2O \quad (16)$$

$$Ca^{2+} +$$

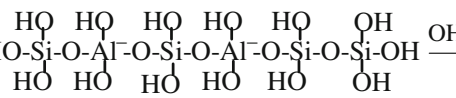

$$\xrightarrow{OH^-}$$

$$CaAl_2Si_4O_{12}\,2H_2O + 5H_2O \quad (17)$$

(6) Production of natrolite The polycondensation takes place among three molecular $Si(OH)_4$ and two molecular $Al^-(OH)_4$ to form the pentamer including three Si and two Al atoms in reaction (18), and then the pentamer reacts with Na^+ to produce natrolite exhibited in reaction (19).

$$3Si(OH)_4 + 2Al^-(OH)_4 \xrightarrow{OH^-}$$

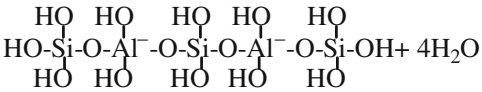

$$+ 4H_2O \quad (18)$$

$$2Na^+ +$$

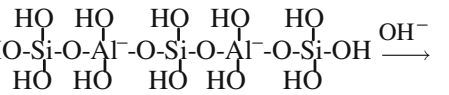

$$\xrightarrow{OH^-}$$

$$Na_2Al_2Si_3O_{10}\,2H_2O + 4H_2O \quad (19)$$

(7) Production of clinozoisite Even though the chemical composites of clinozoisite is same as zoisite, their crystal structures are different, that is, clinozoisite belongs to the monoclinic system and the zoisite is of the cubic system. Because the reaction process for the formation of clinozoisite is similar as that of zoisite, the chemical equation is not described here.

The hydration products of geopolymer with amorphous alumino-silicate structures and mineral phases with analogies to natural zeolites have been generated by alkaline activation of GBFS in the different curing ages from initial setting time to 28d in this paper. It is well-known that the alkaline activations of cementitious materials as new cements have better durability than that of OPC due to their zeolite-like structure feature [6–8]. In our cases, the structural stability and durability of erosion resistance of carbonate were further tested using XRD and FTIR after the sample was naturally placed at room temperature for 18 months. It was found that the pattern of XRD is similar to that of the sample at the curing time of 28d in Fig. 2 suggesting that the structure of sample is considerably stable. At the same time, the sample was divided into two parts to carry out FTIR analysis, one part is from the surface layer and the other is from the interior. The results indicated that the surface layer appears a band of C–O stretching vibration proposing that the shallow surface layer of the sample was eroded by carbonates in atmosphere, but the interior of sample does not find any infrared absorption band of C–O bond.

Conclusion

The hydration mechanism of geopolymers synthesized by alkaline activation of GBFS in different curing ages is studied by the XRD and FTIR. The XRD results reveal that some new mineral phases are produced, for instance, calcium silicate hydrate, tobermolite, gismondine, zoisite, wairakite natrolite, and clinozoisite, respectively, in the curing times from 1d to steam curing time of 28d. The FTIR results provide that the new vibration bands at around 671.2 cm^{-1} and 714.0 cm^{-1} are the evidences for the formation of Si–O–Al framework structure in the curing age from 1d to 28d. The hydration mechanism of geopolymer formed by waterglass activation of GBFS is via waterglass hydrolysis, cleavage of glassy network structure, production of geopolymers by polycondensation, and formation of new mineral phases through aluminosilicate oligomers reacting with Ca^{2+} and Na^+ ions under OH^- catalysis.

Acknowledgements The authors gratefully acknowledge the financial support from the Specialized Research Fund for the Doctoral Program of Higher Education (SRFDP) (No. 20050698034) and the Project Sponsored by the Scientific Research Foundation for the Returned Overseas Chinese Scholars, State Education Ministry (No. 200555).

References

1. Duxson P, Provis JL, Lukey GC, Van Deventer JSJ (2007) Cem Concr Res 37:1590

2. Glukhovsky VD (1959) Soil silicates. Gosstroyizdat USSR, Kiev, in Russian
3. Krivenko PV, Skurchinskaya J (1991) In: Proceedings of the international conference on the utilization of fly ash and other coal combustion by-products, Shanghai, pp 64.1–64.7
4. Krivenko PV, Kovalchuk GY (2002) Innovations and developments in concrete materials and construction. In: proceedings of the international conference on challenges of concrete construction, Dundee, pp 123–132
5. Usherov-Marshak AV, Krivenko PV, Pershina LA (1998) Cem Concr Res 28(9):1289
6. Khate D, Chaudhary R (2007) J Mater Sci 42:729. doi:10.1007/s10853-006-0401-4
7. Komnitsas K, Zaharak D (2007) Miner Eng 20:1261
8. Duxson P, Fernandez-Jimenez A, Provis JL, Lukey GC, Palomo A, Van Deventer JSJ (2007) J Mater Sci 42:2917. doi:10.1007/s10853-006-0637-z
9. Roy DM (1999) Cem Concr Res 29:249
10. Van Deventer JSJ, Provis JL, Duxson P, Lukey GC (2007) J Hazard Mater 139:506
11. Krivenko PV, Kovalchuk GY (2007) J Mater Sci 42:2944. doi:10.1007/s10853-006-0528-3
12. Davidovits J (1991) J Therm Anal 37:1633
13. Pereira CF, Luna Y, Querol X, Antenucci D, Vale J (2008) Waste stabilization/solidification of an electric arc furnace dust using fly ash-based geopolymers. Fuel. doi:10.1016/j.Fuel.2008.01.021
14. Panagiotopoulou Ch, Kontori E, Perraki Th, Kakali G (2007) J Mater Sci 42:2967. doi:10.1007/s10853-006-0531-8
15. Yip CK, Lukey GC, Van Deventer JSJ (2005) Cem Concr Res 35:1688
16. Yip CK, Lukey GC, Van Deventer JSJ (2004) Ceram Trans 153:187
17. Yip CK, Van Deventer JSJ (2003) J Mater Sci 38:3851. doi:10.1023/A:1025904905176
18. Cheng TW, Chiu JP (2003) Miner Eng 16:205
19. Song S, Sohn D, Jennings HM, Mason TO (2000) J Mater Sci 35:249. doi:10.1023/A:1004742027117
20. Sagoe-Crentsil K, Weng L (2007) J Mater Sci 42:3007. doi:10.1007/s10853-006-0818-9
21. Schneider J, Cincotto MA, Panepucci H (2001) Cem Concr Res 31:993
22. Bakharev T (2005) Cem Concr Res 35:658
23. Feng D, Tan H, Van Deventer JS (2004) J Mater Sci 39:571. doi:10.1023/B:JMSC.0000011513.87316.5c
24. Yousuf M, Mollah A, Hess TR, Tsai YN, Cocke DL (1993) Cem Concr Res 23:773
25. Perera DS, Uchida O, Vance ER, Finnie KS (2007) J Mater Sci 42:3099. doi:10.1007/s10853-006-0533-6
26. Lee WKW, Van Deventer JSJ (2002) Colloids Surf A Physicochem Eng Asp 211:115
27. Weng L, Sagoe-Crentsil K (2007) J Mater Sci 42:2997. doi:10.1007/s10853-006-0820-2
28. Silva PD, Sagoe-Crenstil K, Sirivivatnanon V (2007) Cem Concr Res 37:512